Pis'ma v ZhETF, vol. 95, iss. 6, pp. 310 – 316 © 2012 March 25

Cylindrical and spherical electron-acoustic Gardner solitons and double layers in a two-electron-temperature plasma with nonthermal ions

S. T. Shuchy[1)], *A. Mannan*, *A. A. Mamun*

Department of Physics, Jahangirnagar University, Savar, Dhaka-1342, Bangladesh

Submitted 19 January 2012

Cylindrical and spherical Gardner solitons (GSs) and double layers (DLs) in a two-electron-temperature plasma system (containing cold electrons, hot electrons obeying a Boltzmann distribution, and hot ions obeying a nonthermal distribution) are studied by employing the reductive perturbation method. The modified Gardner (MG) equation describing the nonlinear propagation of the electron-acoustic (EA) waves is derived, and its nonplanar GS- and DL-solutions are numerically analyzed. The parametric regimes for the existence of GSs, which are associated with both positive and negative potential, and DLs which are associated with positive potential, are obtained. The basic features of nonplanar EA GSs, and DLs, which are found to be different from planar ones, are also identified. The implications of our results in space and laboratory plasmas are briefly discussed.

1. Introduction. The idea of electron-acoustic (EA) mode had been conceived by Fried and Gould [1] during numerical solutions of the linear electrostatic Vlasov dispersion equation in an unmagnetized, homogenous plasma. It is basically an acoustic-type of waves [2] in which the inertia is provided by the cold electron mass, and the restoring force is provided by the hot electron thermal pressure. The ions play the role of a neutralizing background only. The spectrum of the linear EA-waves, unlike that of the well-known Langmuir waves, extends only up to the cold electron plasma frequency $\omega_{pc} = (4\pi n_{c0} e^2/m_e)^{1/2}$, where n_{c0} is the unperturbed cold electron number density, e is magnitude of the electron charge, and m_e is the mass of an electron. This upper wave frequency limit ($\omega \simeq \omega_{pc}$) corresponds to a short-wavelength EA-wave and depends on the unperturbed cold electron number density n_{c0}. On the other hand, the dispersion relation of the linear EA-waves in the long-wavelength limit (in comparison with the hot electron Debye radius $\lambda_{dh} = (k_{\rm B} T_h/4\pi n_{h0} e^2)^{1/2}$, where T_h is the hot electron temperature, $k_{\rm B}$ is the Boltzmann constant, and n_{h0} is the unperturbed hot electron number density) is $\omega \simeq kC_e$, where k is the wave number and $C_e = (n_{c0} k_{\rm B} T_h/n_{h0} m_e)^{1/2}$ is the EA speed [3]. Besides the well-known Langmuir and ion-acoustic waves, they noticed the existence of a heavily damped acoustic-like solution of the dispersion equation. It was later shown that in the presence of two distinct groups (cold and hot) of electrons and immobile ions, one indeed obtains a weakly damped EA-mode [2], the properties of which significantly differ from those of the Langmuir waves. Gary and Tokar [3] performed a parameter survey and found conditions for the existence of the EA-waves. The most important condition is $T_c \ll T_h$, where T_c (T_h) is the temperature of cold (hot) electrons. The propagation characteristics of the EA-waves have also been studied by Yu and Shukla [4], Mace and Hellberg [5–7] and Mace et al. [8].

Two-electron-temperature plasmas are known to occur both in laboratory experiments [9, 10] and in space environments [11–17]. The propagation of the EA-waves has received a great deal of renewed interest not only because the two-electron-temperature plasma is very common in laboratory experiments and in space, but also because of the potential importance of the EA-waves in interpreting electrostatic component of the broadband electrostatic noise (BEN) observed in the cusp of the terrestrial magnetosphere [12, 18], in the geomagnetic tail [19], in auroral region [11, 13, 15], etc.

The EA-mode has been used to explain various wave emissions in different regions of the Earth's magnetosphere [11, 15]. It was first applied to interpret the hiss emissions observed in the polar cusp region in association with low-energy ($\sim 100\,$eV) upward moving electron beams [20]. The EA-mode was also utilized to interpret the generation of the BEN-emissions detected in the plasma sheath [19] as well as in the dayside auroral zone [11, 15]. Dubouloz et al. [11] rigorously studied the BEN observed in the dayside auroral zone and showed that because of the very high electric field amplitudes (100 mV/m) involved, the nonlinear effects must play a significant role in the generation of the BEN in the dayside auroral zone. Dubouloz et al. [11, 15] also explained the short-duration ($< 1s$) burst of the BEN in terms of electron acoustic solitary waves (EA-SWs):

[1)] e-mail: shuchy_phys@yahoo.com

such EA-SWs passing the satellite would generate electric field spectra. To study the properties of EA solitary structures, Dubouloz et al. [11] considered a one-dimensional, unmagnetized collisionless plasma consisting of cold electrons, Maxwellian hot electrons, and stationary ions. El-Shewy [21] has investigated the propagation of linear and nonlinear EA-SWs in a plasma containing cold electrons, nonthermal hot electrons, and stationary ions. The effects of arbitrary amplitude EA-SWs and electron acoustic double layers (EA-DLs) in a plasma consisting of cold electrons, superthermal hot electrons, and stationary ions has been considered by Sahu [22]. The EA-SWs in a two-electron-temperature plasma where ions form stationary charge neutral background has been observed by Dutta [23]. El-Wakil et al. [24] considered cold electrons, nonthermal hot electrons, and stationary ions, and studied the nonlinear properties of EA-SWs by using time-fractional Korteweg-de Vries (K-dV) equation. However, all of these studies [9–15, 17, 21–24] are limited to one-dimensional ($1D$) planar geometry, which may not be the realistic situation in space and laboratory devices, since the waves observed in space (laboratory devices) are certainly not infinite (unbounded) in one-dimension [25]. Thus, there are some space, where the energetic ions are observed. The energetic ions are described by a new distribution called nonthermal distribution [26–28]. The latter is now being common feature of the Earth's atmosphere and in general it is turning out to be a characteristic feature of space plasmas [29]. To the best of our knowledge no attempt has been made in order to study the effect of nonthermal (energetic or fast) ions on the electron acoustic Gardner solitons (EA-GSs) and EA-DLs. Therefore, in our present work, we consider a plasma system (consisting of cold electrons, hot electrons obeying a Boltzmann distribution, and hot ions following nonthermal distribution) and a more general geometry (which is valid for both planar, cylindrical and spherical geometries), and theoretically study the basic features of the EA-GSs and EA-DLs that are found to exist in such a realistic nonthermal plasma system.

2. Derivation of the MG-equation. We consider a nonplanar (cylindrical or spherical) geometry, and nonlinear propagation of the EA-waves in a nonplanar, collisionless unmagnetized plasma system consisting of cold electrons, hot electrons obeying a Boltzmann distribution, and hot ions obeying a nonthermal distribution. Thus, at equilibrium we have $n_{i0} = n_{h0} + n_{c0}$, where n_{i0} is the nonthermal ion number density at equilibrium. The nonlinear dynamics of the EA-waves propagating in such a nonplanar plasma system is governed by

$$\frac{\partial n_c}{\partial t} + \frac{1}{r^\nu}\frac{\partial}{\partial r}(r^\nu n_c u_c) = 0, \tag{1}$$

$$\frac{\partial u_c}{\partial t} + u_c\frac{\partial u_c}{\partial r} = \frac{\partial \phi}{\partial r}, \tag{2}$$

$$\frac{1}{r^\nu}\frac{\partial}{\partial r}\left(r^\nu \frac{\partial \phi}{\partial r}\right) = -\rho, \tag{3}$$

$$\rho = (1 + \beta\sigma\phi + \beta\sigma^2\phi^2)e^{-\sigma\phi} - \mu e^{\phi} - (1-\mu)n_c, \tag{4}$$

where $\nu = 0$ for $1D$ planar geometry, and $\nu = 1$ (2) for a nonplanar cylindrical (spherical) geometry; n_c is the cold electron number density normalized by its equilibrium value n_{c0}, u_c is the cold electron speed normalized by C_e, ϕ is the wave potential normalized by $k_{\rm B}T_h/e$, ρ is the surface charge density normalized by en_{h0}, $\mu = n_{h0}/n_{i0}$, $\sigma = T_h/T_i$, T_i is the ion temperature, and $\beta = 4\alpha/(1+3\alpha)$ in which α is the nonthermal parameter [26–28]. The time variable t is normalized by ω_{pc}^{-1}, and the space variable r is normalized by λ_{dh}.

To study finite amplitude EA-GSs and EA-DLs by the reductive perturbation method [30, 31], we first introduce the stretched coordinates:

$$\zeta = \epsilon(r - V_p t), \tag{5}$$

$$\tau = \epsilon^3 t, \tag{6}$$

where ϵ is a small parameter ($0 < \epsilon < 1$) measuring the weakness of the dispersion, and V_p (normalized by C_e) is the phase speed of the perturbation mode, and expand all the dependent variables (viz. n_c, u_c, ϕ, and ρ) in power series of ϵ:

$$n_c = 1 + \epsilon n_c^{(1)} + \epsilon^2 n_c^{(2)} + \epsilon^3 n_c^{(3)} + \cdots, \tag{7}$$

$$u_c = 0 + \epsilon u_c^{(1)} + \epsilon^2 u_c^{(2)} + \epsilon^3 u_c^{(3)} + \cdots, \tag{8}$$

$$\phi = 0 + \epsilon\phi^{(1)} + \epsilon^2\phi^{(2)} + \epsilon^3\phi^{(3)} + \cdots, \tag{9}$$

$$\rho = 0 + \epsilon\rho^{(1)} + \epsilon^2\rho^{(2)} + \epsilon^3\rho^{(3)} + \cdots. \tag{10}$$

Now, expressing (1)–(4) in terms of ζ and τ by using (5), (6), and substituting (7)–(10) into the resulting equations, one can easily develop different sets of equations in various powers of ϵ. To the lowest order in ϵ one obtains

$$u_c^{(1)} = -\frac{\psi}{V_p}, \quad n_c^{(1)} = -\frac{\psi}{V_p^2}, \tag{11}$$

$$\rho^{(1)} = 0, \quad V_p^2 = \frac{1-\mu}{\mu + \sigma(1-\beta)}, \tag{12}$$

where $\psi = \phi^{(1)}$. The expression for V_p in (12) represents the linear dispersion relation for the EA-waves propagating in a plasma under consideration. To the next higher order in ϵ, we obtain another set of equations, which, after using (11), (12), can be simplified as

$$u_c^{(2)} = \frac{\psi^2}{2V_p^3} - \frac{\phi^{(2)}}{V_p},\ n_c^{(2)} = \frac{3\psi^2}{2V_p^4} - \frac{\phi^{(2)}}{V_p^2}, \tag{13}$$

$$\rho^{(2)} = \frac{1}{2}A\psi^2 = 0,\ A = \sigma^2 - \mu - \frac{3}{V_p^4}(1-\mu). \tag{14}$$

It is obvious from (14) that $A = 0$, since $\psi \neq 0$. The solution of $A = 0$ for α is given by

$$\alpha = \alpha_c = \frac{6(\sigma^2-\mu^2) + 3\mu(1+\sigma)^2 \pm 4\sigma\eta}{18\mu^2 + 9\mu(\sigma-1)^2 - 6\sigma^2}, \tag{15}$$

where $\eta = \sqrt{3(\mu-1)(\mu-\sigma^2)}$. We have numerically shown how α_c varies with μ and σ. The result is displayed in Fig. 1 which, in fact, represents the $A = 0$ surface plot, and provides us the parametric regimes (which correspond to above or below the $A = 0$ surface plot) of our present interest. So, for α around its critical value (α_c), i.e. for $|\alpha - \alpha_c| = \epsilon$ corresponding to $A = A_0$, we can express A_0 as

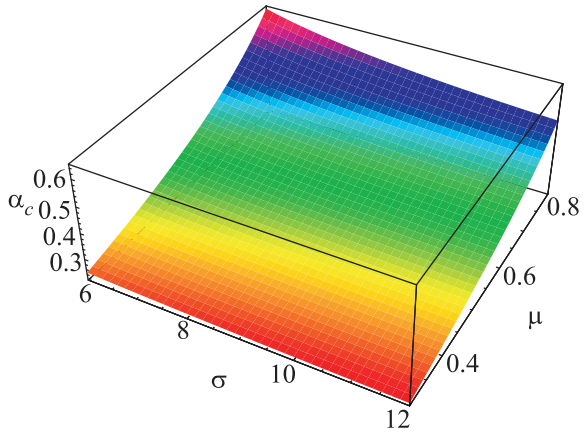

Fig. 1. (Color online) Showing how α_c varies with σ and μ for $A(\alpha = \alpha_c) = 0$

$$A_0 \simeq s\left(\frac{\partial A}{\partial \alpha}\right)_{\alpha=\alpha_c} |\alpha - \alpha_c| = sA_\alpha\epsilon, \tag{16}$$

where

$$A_\alpha = \frac{-24\sigma(\mu + 3\alpha_c\mu + \sigma - \alpha_c\sigma)}{(1+3\alpha_c)^3(\mu-1)}, \tag{17}$$

and $s = 1$ for $\alpha > \alpha_c$ and $s = -1$ for $\alpha < \alpha_c$. So, for $\alpha \neq \alpha_c$, we can express $\rho^{(2)}$ as

$$\rho^{(2)} \simeq \frac{1}{2}s\epsilon A_\alpha\psi^2. \tag{18}$$

This means that for $\alpha \neq \alpha_c$, $\rho^{(2)}$ must be included in the third order Poisson's equation. To the next higher order in ϵ, we obtain the third set of equations:

$$\frac{\partial n_c^{(1)}}{\partial\tau} + \frac{\nu u_c^{(1)}}{V_p\tau} - V_p\frac{\partial n_c^{(3)}}{\partial\zeta} + \frac{\partial F_c}{\partial\zeta} = 0, \tag{19}$$

$$\frac{\partial u_c^{(1)}}{\partial\tau} - V_p\frac{\partial u_c^{(3)}}{\partial\zeta} + \frac{\partial}{\partial\zeta}\left[u_c^{(1)}u_c^{(2)}\right] - \frac{\partial\phi^{(3)}}{\partial\zeta} = 0, \tag{20}$$

$$\frac{\partial^2\psi}{\partial\zeta^2} + \frac{1}{2}sA_\alpha\psi^2 - (\mu+\sigma-\beta\sigma)\phi^{(3)} - (\mu-\sigma^2)\psi\phi^{(2)} - (1-\mu)n_c^{(3)} - \left(\frac{\mu}{6} + \frac{\beta\sigma^3}{2} + \frac{\sigma^3}{6}\right)\psi^3 = 0, \tag{21}$$

where $F_c = n_c^{(1)}u_c^{(2)} + n_c^{(2)}u_c^{(1)} + u_c^{(3)}$. Now, using (11)–(14) and (19)–(21), we finally obtain a nonlinear dynamical equation of the form:

$$\frac{\partial\psi}{\partial\tau} + \frac{\nu}{2\tau}\psi + p\psi\frac{\partial\psi}{\partial\zeta} + q\psi^2\frac{\partial\psi}{\partial\zeta} + p_0\frac{\partial^3\psi}{\partial\zeta^3} = 0, \tag{22}$$

where $p = sA_\alpha p_0$, $q = p_0q_0$, and

$$p_0 = \frac{V_p^3}{2(1-\mu)}, \tag{23}$$

$$q_0 = \frac{15}{2V_p^6}(1-\mu) - \frac{1}{2}[\mu + (1+3\beta)\sigma^3]. \tag{24}$$

Equation (22) is a modified Gardner (MG) equation. The modification is due to the extra term, $(\nu/2\tau)\psi$, which arises due to the effects of the nonplanar geometry. We have already mentioned that $\nu = 0$ corresponds to a $1D$ planar geometry which reduces (22) to a standard Gardner (SG) equation.

3. Numerical analysis. We have already mentioned that $\nu = 0$ corresponds to a $1D$ planar geometry which reduces (22) to a standard Gardner (SG) equation. Before going to numerical solutions of MG-equation, we will first analyze stationary GSs-solution [32] of this SG-equation (22) (with $\nu = 0$). To do so, we first introduce a transformation $\xi = \zeta - U_0\tau$ which allows us to write (22), under the steady state condition, as

$$\frac{1}{2}\left(\frac{d\psi}{d\xi}\right)^2 + V(\psi) = 0, \tag{25}$$

where the pseudo-potential $V(\psi)$ is

$$V(\psi) = -\frac{U_0}{2p_0}\psi^2 + \frac{sA_\alpha}{6}\psi^3 + \frac{q_0}{12}\psi^4. \tag{26}$$

It is obvious from (26) that

$$V(\psi)\,|_{\psi=0} = \left.\frac{dV(\psi)}{d\psi}\right|_{\psi=0} = 0, \tag{27}$$

$$\left.\frac{d^2V(\psi)}{d\psi^2}\right|_{\psi=0} < 0. \tag{28}$$

The conditions (27) and (28) imply that the solitary wave (SW) solution of (25) exist if

$$V(\psi)|_{\psi=\psi_m} = 0. \tag{29}$$

The latter can be solved as

$$U_0 = \frac{p}{3}\psi_{m1,2} + \frac{q}{6}\psi_{m1,2}^2, \tag{30}$$

$$\psi_{m1,2} = \psi_m \left(1 \mp \sqrt{1 + U_0/V_0}\right), \tag{31}$$

where $\psi_m = -sA_\alpha/q_0$ and $V_0 = A_\alpha^2 s^2 p_0/6q_0$. Now, using (26) and (31) in (25), we have

$$\left(\frac{d\psi}{d\xi}\right)^2 + \gamma\psi^2(\psi - \psi_{m1})(\psi - \psi_{m2}) = 0, \tag{32}$$

where $\gamma = q_0/6$. The stationary SW-solution of the SG-equation (i.e. (22) with $\nu = 0$) can be written as

$$\psi = \left[\frac{1}{\psi_{m2}} - \left(\frac{1}{\psi_{m2}} - \frac{1}{\psi_{m1}}\right)\cosh^2\frac{\xi}{\delta}\right]^{-1}, \tag{33}$$

where $\psi_{m1,2}$ is given in (31), and δ is the width of the solitary waves (SWs), and is given by

$$\delta = \sqrt{-\frac{4}{\gamma\psi_{m1}\psi_{m2}}} = \sqrt{\frac{p_0}{U_0}}. \tag{34}$$

We note that (33) represents a SW-solution of (22) with $\nu = 0$. It is, therefore, obvious that, to have GSs we must have $U_0 < V_0$, otherwise $\psi_{m1,2}$ become imaginary. It is clear from Eqs. (14) that the solitary potential profile is positive (negative) if $A > 0$ ($A < 0$). Therefore, $A(\alpha = \alpha_c) = 0$, where α_c is the critical value of α above (below) which the SWs with a positive (negative) potential exists, gives the value of α_c. To find the parametric regimes for which the positive and negative solitary potential profiles exist, we have numerically analyzed A, and obtain $A(\alpha = \alpha_c) = 0$ surface plot. The $A(\alpha = \alpha_c) = 0$ surface plot is shown in Fig. 1. We have the existence of the small amplitude SWs with a negative potential for $\alpha < \alpha_c$ shown in Figs. 3 and 5 and with a positive potential for $\alpha > \alpha_c$ shown in Figs. 2 and 4.

The stationary DL-solution of the SG equation (i.e. (22) with $\nu = 0$) is obtained by considering a moving frame (moving with speed U_0) $\xi = \zeta - U_0\tau$, and imposing all the appropriate boundary conditions for DL-solution, including $\psi \to 0$, $d\psi/d\xi \to 0$, $d^2\psi/d\xi^2 \to 0$ at $\xi \to -\infty$. These boundary conditions for the stationary DL-solution [33] allow us to express the SG-equation (i.e., (22) with $\nu = 0$) as

$$\psi = \frac{\psi_m}{2}\left(1 + \tanh\frac{\xi}{\Delta}\right), \tag{35}$$

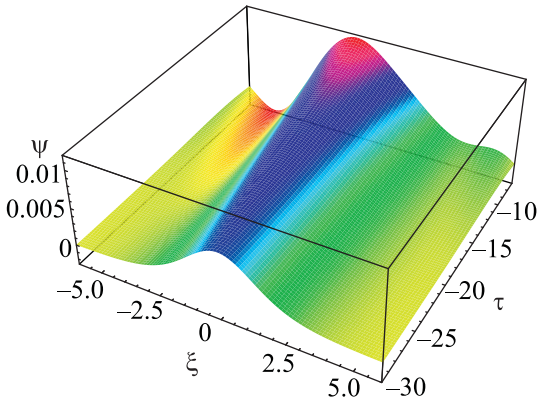

Fig. 2. (Color online) Showing the effects of cylindrical geometry on EA positive GSs for $\mu = 0.5$, $\sigma = 10$, $\alpha = 0.32$, and $U_0 = 0.05$

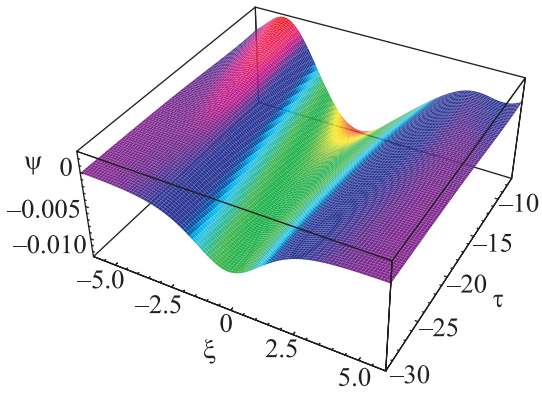

Fig. 3. (Color online) Showing the effects of cylindrical geometry on EA negative GSs for $\mu = 0.5$, $\sigma = 10$, $\alpha = 0.30$, and $U_0 = 0.05$

where the amplitude (ψ_m) and the width (Δ) of the DLs, and U_0 are given by

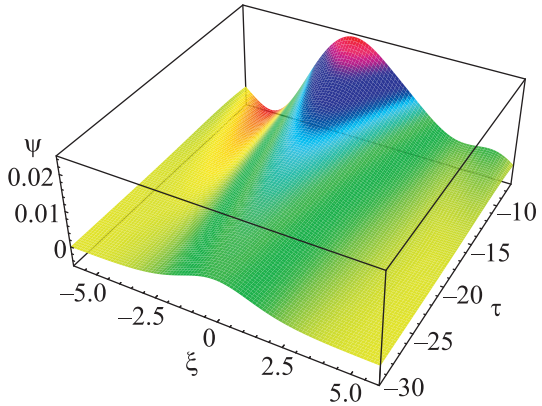

Fig. 4. (Color online) Showing the effects of spherical geometry on EA positive GSs for $\mu = 0.5$, $\sigma = 10$, $\alpha = 0.32$, and $U_0 = 0.05$

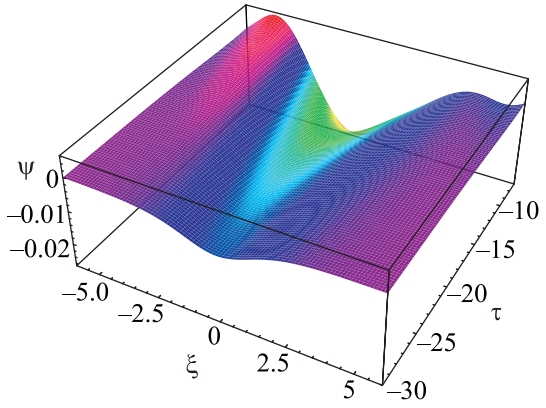

Fig. 5. (Color online) Showing the effects of spherical geometry on EA negative GSs for $\mu = 0.5$, $\sigma = 10$, $\alpha = 0.30$, and $U_0 = 0.05$

$$\psi_m = s\frac{6U_0}{A_\alpha p_0}, \quad \Delta = \sqrt{-\frac{24}{\psi_m^2 q_0}}, \quad U_0 = -\frac{s^2 A_\alpha^2 p_0}{6q_0}. \quad (36)$$

It is clear from (35) and (36) that DLs exist if and only if $q_0 < 0$, i.e. $\alpha > \alpha_D$, where α_D, is represented by the $q_0 = 0$ surface plot, shown in Fig. 2. On the other hand, since $p_0 > 0$ and $U_0 > 0$, (35) and (36) indicate that the DLs are associated with positive potential if $s = 1$, i.e. $\alpha > \alpha_c$, and associated with positive potential if $s = -1$, i.e. $\alpha < \alpha_c$. It is obvious from Figs. 7 and 8 that $\alpha > \alpha_D > \alpha_c$ which confirm us that DLs are associated with positive potential only. The parametric regimes for the existence of positive DLs are represented by the upper surface plot of Fig. 6, and DLs exist for

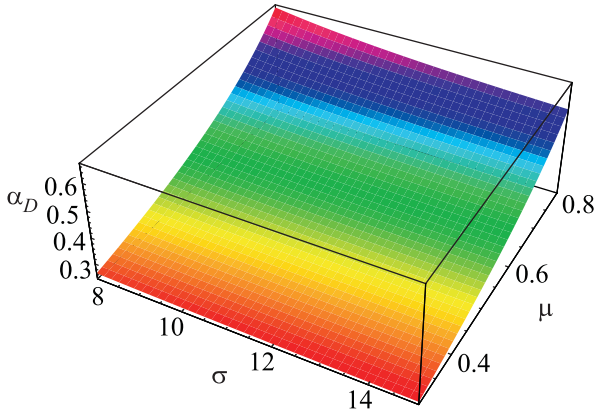

Fig. 6. (Color online) Showing how α_D (obtained from $q_0(\alpha = \alpha_D) = 0$) varies with σ and μ

parameters corresponding to any point above ($q_0 = 0$) surface plot.

We now turn to (22) with the term $(\nu/2\tau)\psi$, which is due to the effects of the nonplanar geometry. An exact analytic solution of (22) is not possible. Therefore, we

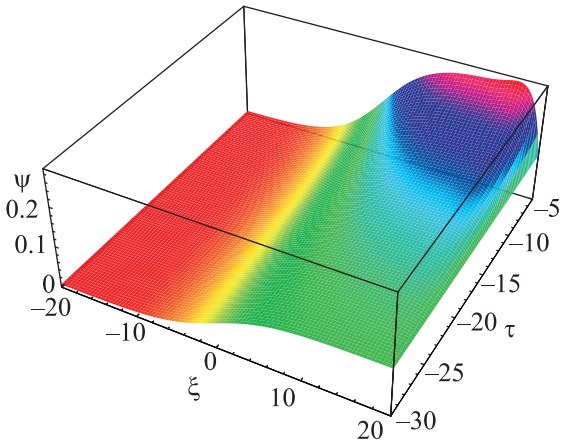

Fig. 7. (Color online) Showing the effects of cylindrical geometry on EA positive DLs for $\alpha = 0.35$, $\mu = 0.5$, $U_0 = 0.5$, and $\sigma = 10$

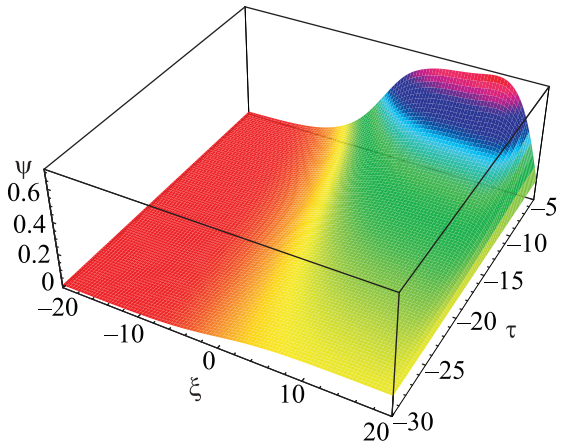

Fig. 8. (Color online) Showing the effects of spherical geometry on EA positive DLs for $\alpha = 0.35$, $\mu = 0.5$, $U_0 = 0.5$, and $\sigma = 10$

have numerically solved (22), and have studied the effects of the nonplanar geometry on time-dependent EA-GSs and EA-DLs. The results are depicted in Figs. 1–8. The initial condition, that we have used in our numerical analysis, is in the form of the stationary solution of (22) without the term $(\nu/2\tau)\psi$. Figs. 2 (4) and 3 (5) show how the effects of a cylindrical (spherical) geometry modify the EA-GSs. Figs. 7 (8) shows how the effects of cylindrical (spherical) geometry modify the EA-DLs for $\alpha = 0.32$, $\mu = 0.5$, $\sigma = 10$, and $U_0 = 0.5$. The numerical solutions of (22) reveal that for a large value of τ (e.g., $\tau = -30$), the spherical and cylindrical geometry of both SWs and DLs are similar to $1D$-structures. This is because for a large value of τ the term $(\nu/2\tau)\psi$, which is due to the effects of the cylindrical ($\nu = 1$) or spherical ($\nu = 2$) geometry, is no longer dominant. However, as the value of τ decreases, the term $(\nu/2\tau)\psi$ becomes

dominant, and cylindrical and spherical of both SW- and DL-structures differ from $1D$ ones. It is found that as the value of τ decreases, the amplitude of these localized pulses increases. It is also found that the amplitude of cylindrical EA-SWs and EA-DLs is larger than those of $1D$ ones, but smaller than that of the spherical ones.

4. Discussion. We have considered a nonplanar geometry, and have studied EA-SWs and EA-DLs in an unmagnetized plasma system consisting of cold electrons, Boltzmann hot electrons, and non thermal ions. The reductive perturbation method has been employed in order to derive the MG equation which is valid beyond the K-dV-limit (corresponding to the vanishing of the nonlinear coefficient of the K-dV-equation, i.e. $\alpha \sim \alpha_c$ in our present situation). The results which have been found from the numerical solutions of the MG-equation, can be summarized as follows.

1. The condition $\alpha > \alpha_c$ ($\alpha < \alpha_c$) allows the existence of finite amplitude EA-SWs with positive (negative) potential. We note that $\alpha_c \sim 0.31$ for $\sigma = 10$ and $\mu = 0.5$.

2. The GSs (represented by (33) for planar geometry and steady state condition), are found to be significantly different from the K-dV-solitons (represented in the form of $\mathrm{sech}^2(\xi/\delta)$) which do not exist for $\alpha \sim \alpha_c$.

3. The magnitude of the amplitude of positive and negative GSs decreases with α, but increases with U_0.

4. The width of positive and negative GSs increases with α, but decreases with U_0.

5. The DLs are found to be formed when $\alpha > \alpha_c, \alpha_D$ where α_c and α_D depend on μ and σ, and decrease with the increase of σ, but increase with μ as obvious from Figs. 1 and 6. We note that $\alpha_D = 0.35$, for $\sigma = 10$ and $\mu = 0.5$. The DLs are associated with positive potential for $\alpha > \alpha_D$.

6. The amplitude of the DLs decreases with the increase of α, but increases with U_0.

7. The width of positive DLs decreases with both of α and U_0.

8. The numerical analysis of the MG-equation dictates that for a very large value of τ the nonplanar EA-GSs, and EA-DLs are identical, but the magnitude of the amplitude of both cylindrical and spherical EA-GSs and EA-DLs increases with the decrease of the value of τ.

9. The basic features (viz. amplitude, width, speed, etc.) are significantly modified by the nonthermal ions.

10. The amplitude of the cylindrical EA-SWs and EA-DLs is larger than those of $1D$ ones, but smaller than that of the spherical ones.

We note that our present theory is valid only for small but finite amplitude solitary structures, but not arbitrary amplitude structures. The ranges of different plasma parameters used in this investigation are very wide ($\mu = 0.2-0.9$, $\sigma = 5-15$, and $\alpha = 0.01-0.5$), are relevant to both space [11–15] and laboratory plasmas [9, 10]. Thus, the results of the present investigation should help us to explain the basic features of localized EA perturbations propagating in space and laboratory plasmas.

The research grant for research equipment from the Third World Academy of Sciences (Trieste, Italy) is gratefully acknowledged. The authors are grateful Prof. P.K. Shukla for his invaluable suggestions during the course of this work.

1. B. D. Fried and R. W. Gould, Phys. Fluids **4**, 139 (1961).
2. K. Watanabe and T. Taniuti, J. Phys. Soc. Jpn. **43**, 1819 (1977).
3. S. P. Gary and R. L. Tokar, Phys. Fluids **28**, 2439 (1985).
4. M. Yu and P. K. Shukla, J. Plasma Phys. **29**, 409 (1983).
5. R. L. Mace and M. A. Hellberg, J. Plasma Phys. **43**, 239 (1990).
6. R. L. Mace and M. A. Hellberg, J. Geophys. Res. **98**, 5881 (1993).
7. R. L. Mace and M. A. Hellberg, Phys. Plasmas **8**, 2649 (2001).
8. R. L. Mace, S. Baboolal, R. Bharuthram, and M. A. Hellberg, J. Plasma Phys. **45**, 323 (1991).
9. H. Derfler and T. C. Simonen, Phys. Fluids **12**, 269 (1969).
10. D. Henry and J. P. Treguier, J. Plasma Phys. **8**, 311 (1972).
11. N. Dubouloz, R. Pottelette, M. Malingre, and R. A. Treumann, Geophys. Res. Lett. **18**, 155 (1991).
12. S. V. Singh and G. S. Lakhina, Planet. Space Sci. **49**, 107 (2001).
13. R. Pottelette, R. E. Ergun, R. A. Treumann et al., Geophys. Res. Lett. **26**, 2629 (1999).
14. M. Berthomier, R. Pottelette, M. Malingre, and Y. Khotyainsev, Phys. Plasmas **7**, 2987 (2000).
15. N. Dubouloz, R. A. Treumann, R. Pottelette, and M. Malingre, J. Geophys. Res.: Atmos. **98**, 17415 (1993).

16. A. P. Kakad, S. V. Singha, R. V. Reddya et al., Adv. Space Res. **43**, 1945 (2009).
17. J. S. Pickett, L.-J. Chen, R. L. Mutel et al., Adv. Space Res. **41**, 1666 (2008).
18. R. L. Tokar and S. P. Gary, Geophys. Res. Lett. **11**, 1180 (1984).
19. D. Schriver and M. Ashour-Abdalla, Geophys. Res. Lett. **16**, 899 (1989).
20. C. S. Lin, J. L. Burch, S. D. Shawhan, and D. A. Gurnett, J. Geophys. Res. **89**, 925 (1984).
21. E. K. El-Shewy, Chaos, Solitons & Fractrals **31**, 1020 (2007).
22. B. Sahu, Phys. Plasmas **17**, 122305 (2010).
23. M. Dutta, N. Chakrabarti, R. Roychoudhury, and M. Khan, Phys. Plasmas **18**, 102301 (2011).
24. S. A. El-Wakil, E. M. Abulwafa, E. K. El-Shewy, and A. A. Mahmoud, Phys. Plasmas **18**, 092116 (2011).
25. P. K. Shukla and M. Rosenberg, Phys. Plasmas **6**, 1038 (1999).
26. R. A. Cairns, A. A. Mamun, R. Bingham et al., Geophys. Res. Lett. **22**, 2709 (1995).
27. A. A. Mamun and P. K. Shukla, Phys. Scripta T **98**, 107 (2002).
28. A. A. Mamun, R. A. Cairns, and P. K. Shukla, Phys. Plasmas **3**, 2610 (1996).
29. Y. Futaana, S. Machida, Y. Saito et al., J. Geophys. Res. **108**, 1025 (2003).
30. H. Washimi and T. Taniuti, Phys. Rev. Lett. **17**, 996 (1966).
31. S. Maxon and J. Viecelli, Phys. Rev. Lett. **32**, 4 (1974).
32. A. Mannan and A. A. Mamun, Phys. Rev. E **84**, 026408 (2011).
33. A. A. Mamun and A. Mannan, JETP Lett. **94**, 356 (2011).